Astron. Astrophys. 328, 670–681 (1997)

ASTRONOMY AND ASTROPHYSICS

# Wavelet analysis of solar activity recorded by sunspot groups

**Peter Frick**[1], **Denis Galyagin**[1], **Douglas V. Hoyt**[2], **Elizabeth Nesme-Ribes**[3,⋆], **Kenneth H. Schatten**[4], **Dmitry Sokoloff**[5], **and Viktor Zakharov**[1]

[1] Institute of Continuous Media Mechanics, Korolyov str.1, 614061 Perm, Russia
[2] Research and Data Syatem Corporation, 78 55 Walker Drive, Suite 460, Greenbelt, MD 20770, USA
[3] CNRS URA 326, Observatoire de Paris, 5 Place Janssen, F-92195 Meudon, France
[4] NASA/Goddard Space Flight Center, Gde 914, Greenblelt, MD 20771, USA
[5] Department of Physics, Moscow State University, 119899 Moscow, Russia

Received 22 September 1995 / Accepted 14 May 1996

**Abstract.** The wavelet transform of monthly sunspot group data from 1610 to 1994 is investigated. Only two pronounced peaks corresponding to the Schwabe and the Gleissberg cycles, are present in this transform. The wavelet analysis of the time-series also shows the Maunder and Dalton minima as well as a deviation in the cycle length around 1900. The variations in the periodicity of the main 11 year cycle are studied. We show that all the minima of this cycle occur when the derivative of cycle length as a function of time is negative. Cycles of greater duration are connected with periods of weak solar activity. While the sunspot group number was periodic at the end of the Maunder minimum, it did not seem to follow any periodic behavior during the main part of this minimum. The abrupt transition between normal and Maunder minimum cycles is present in the sunspot group data.

**Key words:** Sun: activity – sunspots – methods: data analysis

## 1. Introduction

Solar activity is a quasi-periodic phenomenon, with a main period of approximately 22 years. This periodicity may not be constant, though. One way of studying the long-term behavior of this cycle is to use the sunspot number as an index of the 11y, or Schwabe, cycle. Wolf (1851) started such a reconstruction last century, providing the so-called Wolf number. However, Wolf did not look up all the existing archives and used different indices (such as the magnetic aurora) to fill in gaps in sunspot observations. Recently, Hoyt and Schatten (1992 a,b) have undertaken a complete re-analysis of the archives, using sunspot groups to reconstruct solar cycles. As a result, a fairly homogeneous sample of monthly sunspot groups is available spanning a 385-year period (Hoyt et al. 1994). The long-term sunspot forecast started at the time of Galileo and became systematic under the French Astronomical School (Picard and La Hire), from 1660 to 1719. From the 18th century onward, this observational program has been pursued by an increasing number of observatories. This long sunspot survey gives us the possibility to analyze solar activity periodicities in detail, in particular, to find out how stable the main period is, what additional periodicities are present, and what connection there may be between solar periodicities and the Maunder minimum.

The simplest technique for investigating periodicities in sunspot data is obviously the Fourier analysis, i.e. the comparison between the record and a sinusoidal signal of a given frequency. However, this method is not best appropriate to correctly interpret the data. The main (11-year) signal is pseudo-periodic, and its amplitude changes by several orders of magnitude over the time interval under consideration. There is another pseudo-periodic signal, referred to as the Gleissberg cycle, the duration of which ($\sim$ 100 years) is only a few times less than the time interval spanned by the whole time-series (four centuries). Furthermore, a straightforward application of the Fourier analysis to such data set may lead to spurious periodicities, especially at low and intermediate frequencies, due to the finite size of the time-series (Ribes et al., 1989).

A few methods have been developed for studying local spectral properties of quasi-periodic signals (time-frequency analysis). The Wigner-Ville algorithm, for example, produces a spectral analysis of an autocorrelation function (Altarac, 1995), and the windowed Fourier transform of Gabor is based on a family of harmonic functions with different frequencies but limited by the constant size of the window. The wavelet technique is more appropriate to the study of quasi-periodic signals. The wavelet transform, in contrast to the Wigner-Ville technique, yields a linear representation of the signal, and in contrast to the Gabor transform, it uses a family of self-similar functions (for comparison and discussion, see Toresanni, 1995). The wavelet analysis is more appropriate than the Fourier technique for denoising the

*Send offprint requests to*: D. Sokoloff
⋆ Deceased on November the 25th, 1996

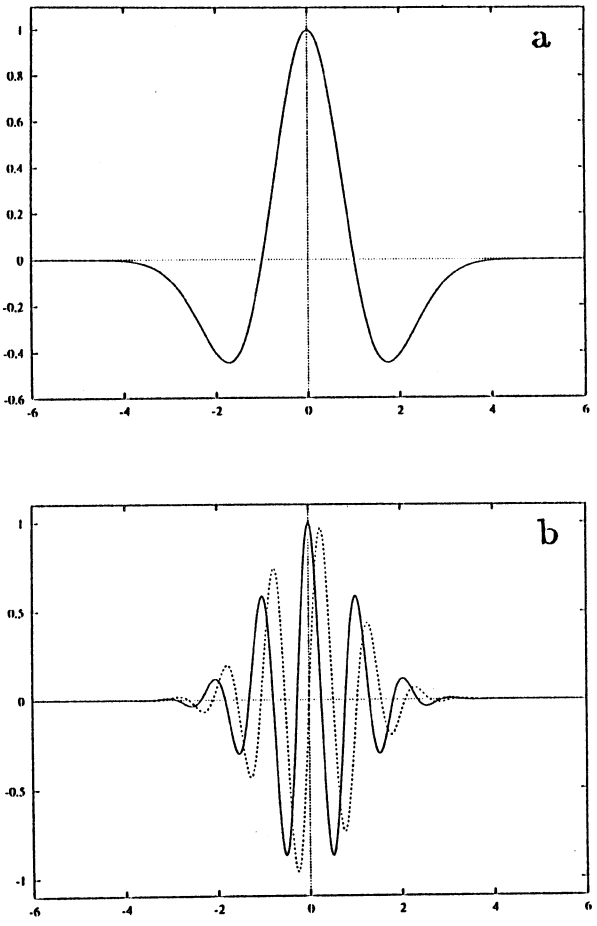


**Fig. 1a and b.** Examples of wavelets: **a** Mexican hat; **b** Morlet wavelet.

signal (see Donoho, 1994); this is appreciable when time-series (like ours) contain observations of uneven quality.

The aim of our paper is to apply wavelet analysis to monthly sunspot group data and discuss the physical results obtained by this technique. Such an analysis was already performed by Ochadlick et al. (1993) using the yearly sunspot data starting from the year 1700. Our study differs from this previous one in that: 1-) Our time-series starts in the early 1600's, including the remarkable event known as the Maunder minimum. 2-) We use monthly sunspot groups rather than yearly means, which seem to be too crude when the averaging time is only 11 times less then the main sunspot period. Because of the time interval spanned, Ochadlick et al. (1993) could hardly make out the Gleissberg cycle. 3-) We also made use of the algorithms developed by Torresani (1995), and applied to the wavelet technique to search for frequency modulation laws in the signal.

Recently, Lawrence et al. (1995) examined daily sunspot data over the last two decades. They obtained the fractal properties of solar activity indicating chaotic behavior at timescales of the order of 1 year, which is much less then the basic period of solar activity. They found that the chaotic behaviour seems to be connected mainly with sunspot formation rather than with solar activity itself. We are interested in longer timescales, so our analysis of monthly sunspot data over four centuries is complementary to that of Lawrence et al. (1995).

## 2. Wavelets

An efficient multi-scale analysis is essential to studying solar activity records. Fourier analysis fails when the time-dependence of scale properties is to be considered. *Wavelet analysis* is more appropriate to a *local* scale analysis with variable resolution. Such a method was developed in the last decade and has already been described in reviews, see e.g. Farge, 1992, and books, see e.g. Meyer, 1992, Daubechies, 1992, Torresani (1995).

Wavelets, unlike sinusoidals, are localized near time $t_0$ and decay if $|t - t_0|$ exceeds the characteristic scale $a$. The wavelet representation can be compared to a kind of mathematical microscope with variable position and magnification. The wavelet transform represents one-dimensional signals as a function of both time and time-scale, and is similar to a local, filtered Fourier transform obtained by expanding and translating the wavelet, and then convolving it with the signal. The windowed Fourier transform contains three parameters (position, scale, frequency), while the wavelet contains two only.

As in the case of the Fourier transform, there are two basic kinds of wavelet transforms: continuous and discrete, that provide orthonormal basis. In this paper we are dealing with the continuous transform, although many of the properties will be valid for both the continuous and the discrete transforms.

### 2.1. What is a wavelet ?

A wavelet's family is generated from a mother wavelet function $\psi(t)$ by translations and dilatations,

$$\psi_{a,b}(t) = a^{-1/2}\psi\left(\frac{t-b}{a}\right) \tag{1}$$

where $a$ and $b$ correspond to the dilatation and the translation respectively.

There are certain requirements in order for the function $\psi(t)$ to be a wavelet. First, the function must have a zero mean (the admissibility condition)

$$\int_{-\infty}^{\infty} \psi(t)dt = 0. \tag{2}$$

Second, the function should be localized in both physical and Fourier space (time and frequency), i.e. its time spread $\Delta t$ and its frequency spread $\Delta\omega$ must satisfy the condition $\Delta t\Delta\omega = const > 2\pi$. In addition, at least one reconstruction formula is needed for reconstructing the signal from its wavelet coefficients and for deducing the energy (or other invariants).

### 2.2. Continuous wavelet transform

The wavelet transform $w(a,t)$ of signal $f(t)$ is defined as

$$w(a,t) = C_\psi^{-1/2} a^{-1/2} \int_{-\infty}^{\infty} \psi^*\left(\frac{t'-t}{a}\right) f(t')dt', \tag{3}$$

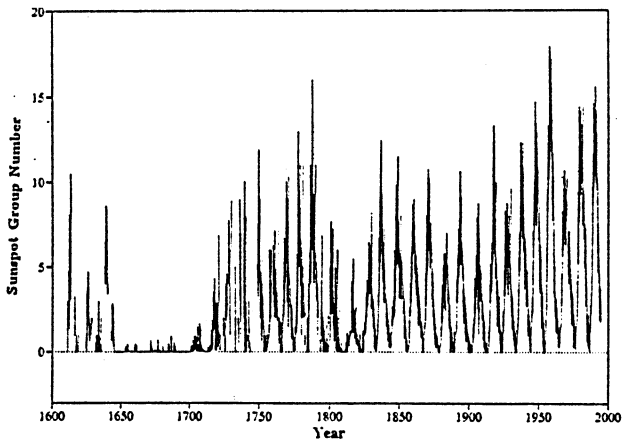


**Fig. 2.** Monthly mean number of sunspot groups (1610 - 1994).

where $\psi(t)$ is a real or complex valued analyzing wavelet, satisfying conditions of subsection *2.1.* and $^*$ stands for complex conjugate.

$$C_\psi = \int_{-\infty}^{\infty} |\omega|^{-1} |\hat{\psi}(\omega)|^2 d\omega \tag{4}$$

and $\hat{\psi}(\omega)$ is the Fourier transform of $\psi(t)$

$$\hat{\psi}(\omega) = \int_{-\infty}^{\infty} \psi(t) e^{-i\omega t} dt. \tag{5}$$

If $C_\psi < \infty$ the wavelet transform can be inverted (Grossmann and Morlet, 1984) as

$$f(t) = C_\psi^{-1/2} \int_0^{\infty} \int_{-\infty}^{\infty} a^{-1/2} \psi\left(\frac{t-t'}{a}\right) w(a,t') \frac{dt'da}{a^2}. \tag{6}$$

One important property of the continuous wavelet transform is a generalization of the Parseval's theorem (Grossmann and Morlet, 1984)

$$\int_{-\infty}^{\infty} f_1(t) f_2^*(t) dt = C_\psi^{-1} \int_0^{\infty} \int_{-\infty}^{\infty} w_1(a,t) w_2^*(a,t) \frac{dtda}{a^2} \tag{7}$$

as a consequence of which the equality is established between energy in physical and wavelet spaces.

The wavelet transform can be also related to the Fourier transform $\hat{f}(\omega)$ of a signal $f(t)$ as

$$w(a,t) = C_\psi^{-1/2} a^{1/2} (2\pi)^{-1} \int_{-\infty}^{\infty} \hat{\psi}^*(a\omega) \hat{f}(\omega) e^{it\omega} d\omega \tag{8}$$

$$\hat{f}(\omega) = C_\psi^{-1/2} \int_0^{\infty} \int_{-\infty}^{\infty} a^{1/2} \hat{\psi}(a\omega) w(a,t) e^{-it\omega} \frac{dtda}{a^2}. \tag{9}$$

We also define the global wavelet spectrum, i.e. the energy contained in all wavelet coefficients of the same scale $a$, as a function of $a$:

$$M(a) = \int |w(a,t)|^2 dt, \tag{10}$$

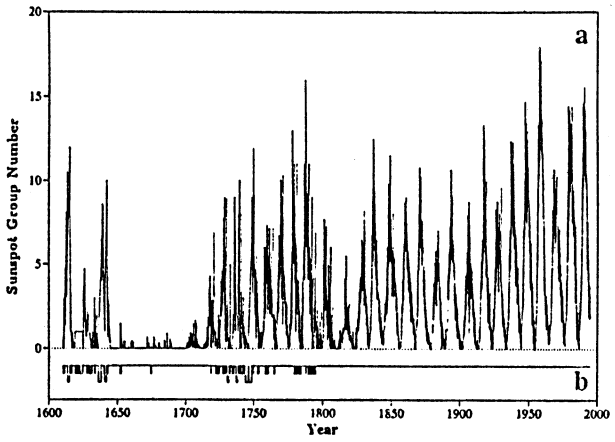


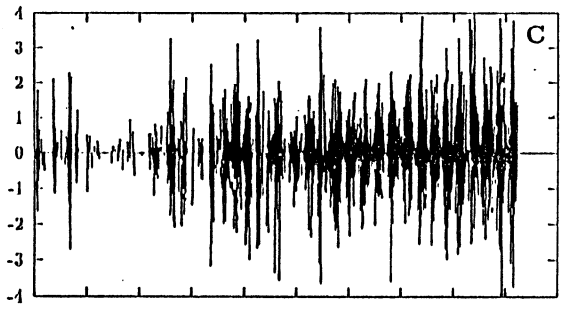


**Fig. 3a–c.** Interpolated monthly mean number of sunspot groups (1610 – 1994); **a** interpolated data, **b** indicator of gaps in data - small negative values correspond to gaps less then 1 year, large ones correspond to gaps longer then 1 year, **c** one example of a statistical noise time-series produced by a generator of white noise using the real dispersion of data

which is related with the Fourier spectrum $E(\omega) = |\hat{f}(\omega)|^2$ as

$$M(a) \sim \int E(\omega) \frac{|\hat{\psi}(a\omega)|^2}{a} d\omega \tag{11}$$

and is actually a smoothed version of Fourier spectrum. Due to the normalization defined in (3), if the Fourier spectrum follows a power law $E(\omega) \sim \omega^\alpha$ the global wavelet spectrum displays the same power law ($M(a) \sim a^{-\alpha}$), as long as the wavelet presents enough cancellation (Perrier et al. 1995).

### *2.3. Some examples*

It is evident that the wavelet representation depends upon the choice of the wavelet $\psi$. Two kinds of wavelets will be used in this paper: the real-valued wavelet, called the "Mexican hat" (Fig. 1a)

$$\psi(t) = (1 - t^2) e^{-t^2/2} \tag{12}$$

and the most widely used complex valued Morlet wavelet (Fig. 1b)

$$\psi(t) = e^{-t^2/2} e^{i\omega_0 t} \tag{13}$$

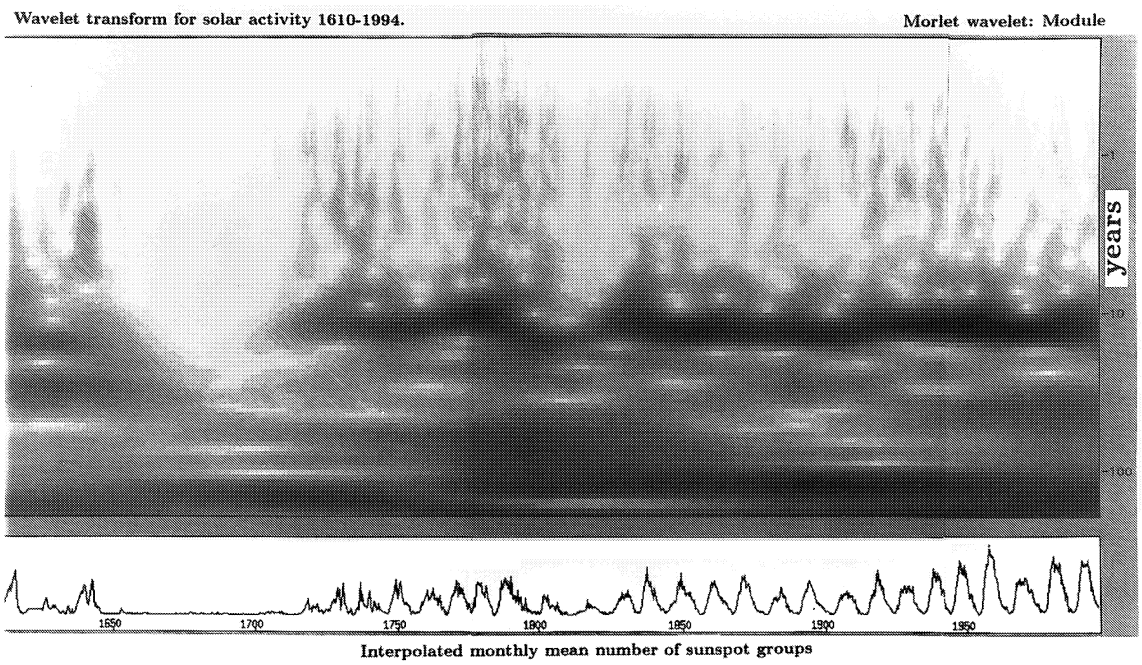


**Fig. 4.** Wavelet transform for solar activity 1610 – 1994; Morlet wavelet modulus.

with $\omega_0 = 6$ (chosen to approximately satisfy the condition (1)). The wavelet technique can be illustrated by canonical examples (see Appendix).

## 3. Monthly sunspot group data

Our data set refers to the sunspot group time-series reconstructed by Hoyt et al. (1994). Details on the reconstruction, the comparison between different observers, the comparison between the Wolf sunspot number can be found in Hoyt and Schatten (1992 a,b) and Hoyt et al. (1994). Let us stress the advantage of using sunspot groups rather than the Wolf number.

A sunspot group has a physical meaning: it is the manifestation of an east-west magnet produced by the stretching of a initial poloidal north-south field under the effect of non uniform solar rotation. In the simplest case, a single magnet appears at a given place, with two sunspots being the poles of the magnets. The Wolf number is defined as ten times the number of sunspot groups plus the number of individual sunspots, with a correction factor depending on the observer. This was done by Wolf in order to smooth out fluctuations. It is evident that the activity index established by Wolf is more empirical.

The time-series he reconstructed is not homogeneous: he used compilations of magnetic aurorae to fill up certain observational gaps. In our case, we used only direct solar observations and we included all 17th century data (Hoyt et al. 1994). Some observational gaps still exist, especially in the mid 18th century. However, our time-series is more complete and homogeneous than Wolf's reconstruction. One may argue that a bias will arise in the time-series due to the improvment of the telescopes since Galilei's time. It has been shown that the bias, if any, would be small and would not change the counts significantly (Ribes and Nesme-Ribes, 1993). By extending the time-series back to the Maunder minimum, we have included the only currently available example of a grand minimum in solar activity. Certain properties of the Maunder minimum have already been discussed by Nesme-Ribes et al. (1994), in terms of the north-south asymmetry of sunspot group number and sunspot rotation. These authors surmised that the onset of the Maunder minimum was fairly rapid. The updated time-series displayed in Fig. 2 clearly shows that the beginning of the Maunder minimum was indeed very abrupt.

Maunder minimum-type events have also been observed in stellar activity by Soon et al. (1994). For those stars entering the Maunder minimum phase, the activity decline is sharp (a transition time comparable with one period of activity). However, stellar information is obviously much noisier than solar data. For example, the contrast between a normal solar activity cycle and the Maunder minimum is about $10^2$ to $10^3$. Such a large contrast could hardly be observed by the stellar magnetic index. Therefore, it is not always clear to what extent one can identify stellar quiet episodes with the solar Maunder minimum. Stellar Maunder minimum-type events should be rather compared with the Dalton minimum observed on the Sun at the end of the 18th century.

The choice of the time-averaging interval is also a relevant question. The lifetime of each sunspot varies from a few hours up to a full solar rotation. The leading sunspot (which appears first on the east limb) is of longer duration than the following one. So a 1-month averaging corresponds to the average lifetime of a sunspot group.

There are a certain number of gaps in the available monthly sunspot group record prior to the 19th century. Assuming that the

lack of sunspot groups over this period was due to a lack of observations, we interpolated to fill these gaps: if isolated months without observations are preceded and followed by months with observations, we apply a linear best fit over four months apart and prescribe the corresponding value to the month without observations. If there is only one month with observation in the center of the gap, we extend the interpolation fit to the next three monthly data. We interpolate gaps of greater than one year with a linear best fit based on eight months of data. In the interpolation process we go from short gaps to longer, basing longer-range interpolations on the shorter.

The longest data gap is about 2.5 years, around 1750, i.e. a period of normal solar activity. This gap is 4.4 times shorter than the main period of solar activity. As similar long-lasting observational gaps are relatively isolated, we believe that our interpolation method does not lead to drastic artificial changes in the data set.

The results of our interpolation are shown in Fig. 3a and informations on time intervals of interpolation and durations are shown in Fig. 3b. Although some uncertainties due to inhomogeneous historical records and observing techniques, the accuracy of the time-series is quite high. It has been shown by Ribes and Nesme-Ribes (1993) that the Maunder minimum was thoroughly observed by Picard and coworkers. So the rapid onset of the Maunder minimum (Figs. 2 and 3a) is likely to be a real phenomenon.

## 4. Results of wavelet analysis

As discussed in Sect. 3, a one-month averaging chosen for performing the wavelet analysis is not completely arbitrary as it corresponds to the average lifetime of a sunspot group. We focussed our wavelet analysis on time-scales larger than the lifetime of individual sunspots.

### *4.1. General structure of solar activity 1610 – 1995*

The general result of the wavelet analysis is presented in Fig. 4 for the whole period 1610-1994. The signal is shown on the lower panel, and the spectral density (modulus of wavelet coefficients) dependence for a given period (vertical axis) and epoch (horizontal axis), in the upper panel. The spectral density corresponds to the intensity of black. Let us consider a given epoch, say 1850. We notice two black layers that are well-pronounced. One corresponds to the Schwabe cycle (11-y cycle), the other to the Gleissberg cycle (about 100 years).

Fig. 5a presents the global wavelet spectrum as a function of the period $T$. For comparison, we also give the Fourier spectrum (Fig. 5b). Because the absolute value of Fourier and Morlet transforms is not very pertinent, we present the result in arbitrary units so that they can be separated on the plot. Both curves show a maximum that is related to the 11-year period (the Schwabe cycle). However, the Fourier transform contains many additional maxima that are mainly data processing artefacts. Only one of the additional maxima survives from the Morlet analysis. This maximum corresponds to a time scale of about 100 years, i.e.

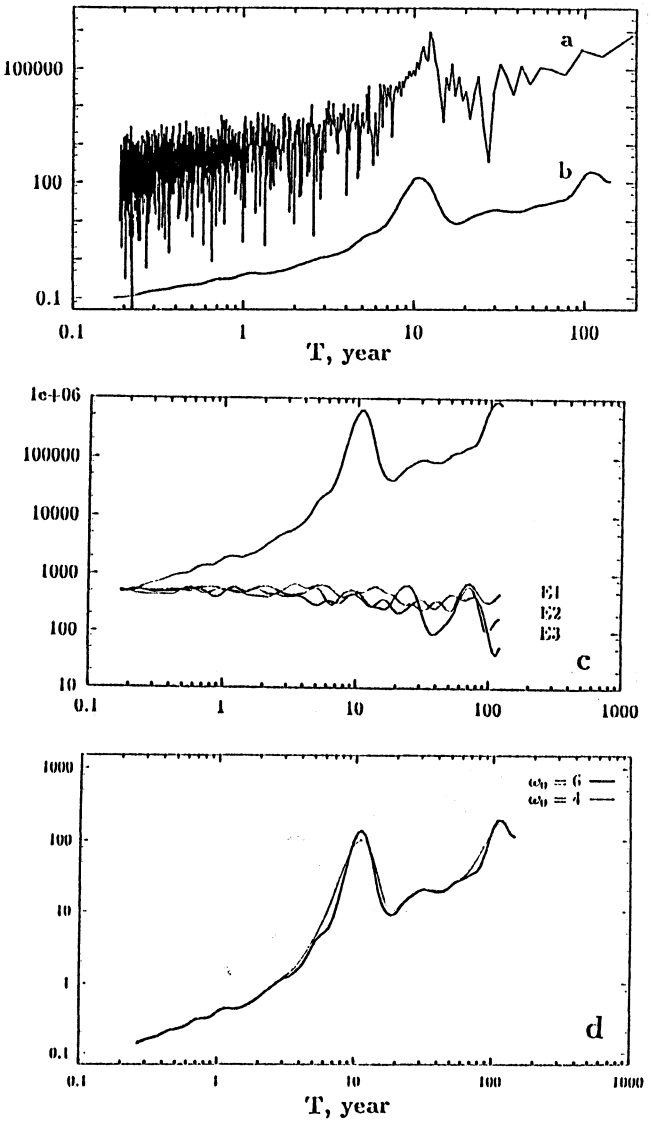


**Fig. 5a–d.** Solar activity spectra; **a** Fourier spectrum, **b** wavelet Morlet spectrum; **c** spectra of errors series generated as white noise with the dispersion of real data; **d** effect of inner frequency in Morlet function on the wavelet spectrum

it can be connected with the so-called Gleissberg cycle. The 11-year power may be connected with a quasi-periodic change of solar activity; the physical meaning of the Gleissberg cycle will be discussed further, with the help of a more sophisticated wavelet analysis.

The spectra in Fig. 5 are plotted on a log-log scale, in which any power-law function produces a linear dependence. Out of the peaks, the Fourier $F(T)$ and Morlet $M(T)$ spectra can be described by some power law functions, $F \sim T^{\alpha}$, $M \sim T^{\beta}$, where $\alpha$ and $\beta$ are estimated from the slope of the linear fit for the corresponding part of the spectrum. One gets $\beta \sim 1$ between maxima and $\beta \sim 3/4$ for $T < 5$ years; $\alpha \sim 1/2$. Such power law-dependencies are typical for stochastic, turbulent motions. However, one should stress that the Fourier spectrum index, $\alpha$,

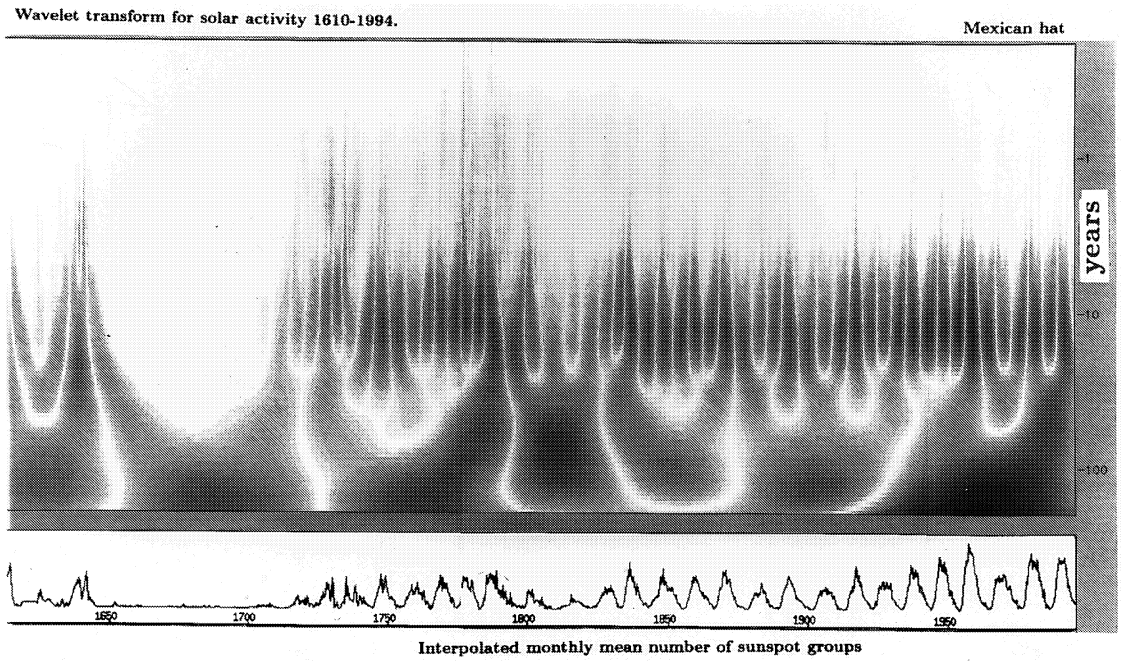


**Fig. 6.** Wavelet transform for solar activity 1610 – 1994; Mexican hat.

is smaller than the corresponding index of the Morlet spectrum, $\beta$. This is because the contribution of noise in the data reduces the spectral index while wavelet transform tends to cleaning the data. A pure white noise would produce a flat spectrum.

To assess the significance of the wavelet signal, we generated several time-series of white noise with the same dispersion as that of the real time-series (three of these time-series are denoted in Fig. 5c as E1, E2, E3). Then we applied the wavelet analysis to the statistical noise time-series. It is clear from Fig. 5c that the wavelet signals present in the real time-series are significant for timescales longer than 1 year.

In contrast with the Fourier analysis, the wavelet result depends on the choice of the wavelet. We used the Mexican hat (12), (see Fig. 1a), and the wavelet coefficients are shown in Fig. 6. The corresponding global spectrum contains the same two peaks, as in the Morlet spectrum. This confirms the robustness of our global wavelet analysis. We also played with the value of $\omega_\circ$ that characterizes the Morlet wavelet: no significant difference is visible on the spectra (Fig. 5d).

### *4.2. Properties of the main cycles*

The Schwabe cycle is visible for almost all epochs except during the deep Maunder minimum (1650 – 1680). The deep Maunder minimum should be considered separately (see below). The Schwabe periodicity is remarkably stable. While the intensity of this 11-year cycle has changed by several orders of magnitude, its duration has changed by several years only, i.e. by 10 % to 20 %. The black layer period corresponding to the Schwabe cycle has finite thickness, i.e. the duration of a given cycle can be estimated only with limited accuracy. However, there are three pronounced deviations of the cycle length present in the time

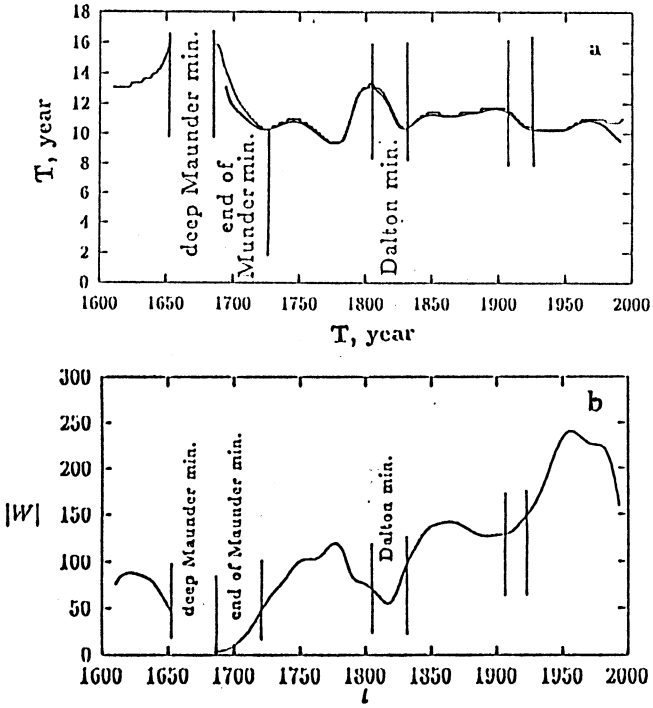


**Fig. 7a and b.** Length (**a**) and cycle strength (**b**) versus time. The thin line on the panel **a** traces the local maximum of wavelet coefficients on the phase plan, and the thick line is obtained by the ridge extraction techniques.

series, one at the end of the Maunder minimum (1680 — 1712), one during the so-called Dalton minimum (1790 — 1820), and one at the beginning of the 20th century, near 1900; the latter event can be compared with the example given in Appendix

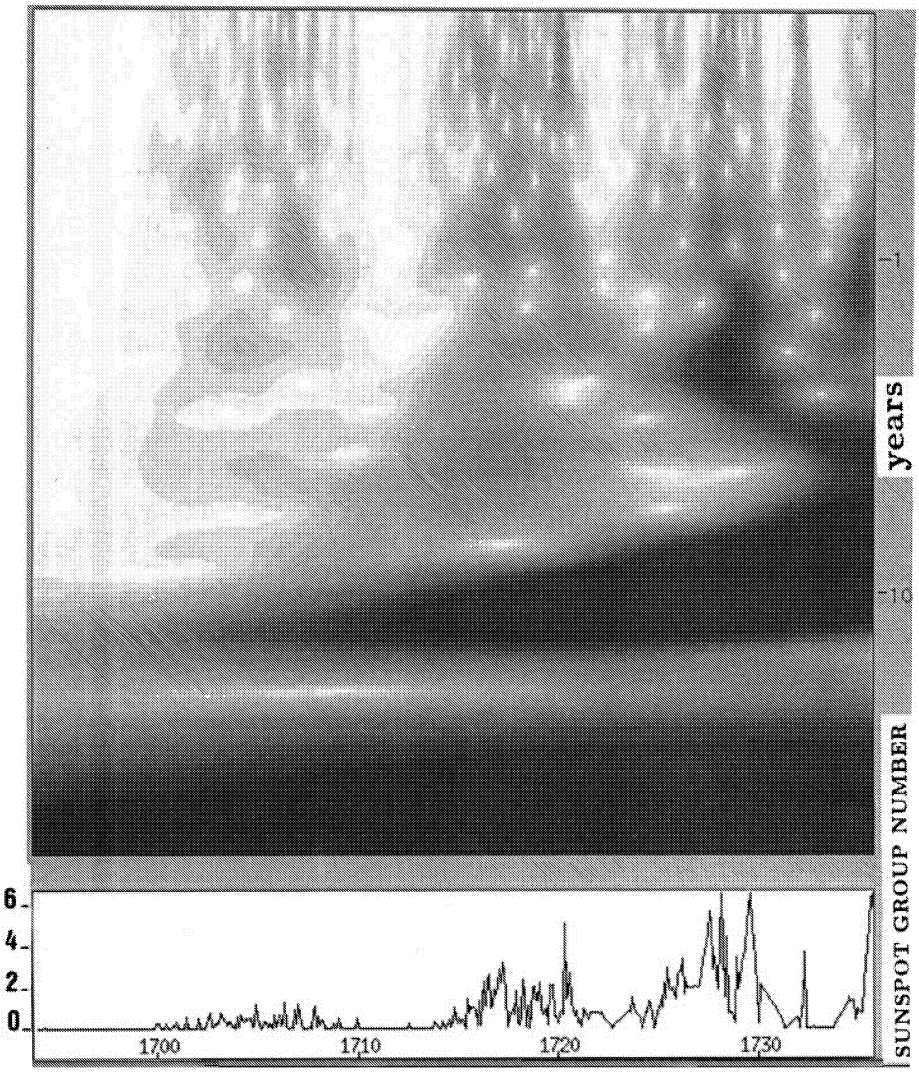


**Fig. 8.** Morlet wavelet transform for the end of the Maunder minimum (1695 – 1737): modulus

(Fig. 12) when there is a change in the length of the cycle. The corresponding Schwabe cycles are also less intensive.

To investigate the time-behavior of the main solar activity cycle in detail, we plotted the time-scale $T$, which corresponds to the maximum spectral intensity at a given time $t$ in the wavelet representation of the 8-16 year band (Fig. 7a). The layer is thick enough but the position of the maximum varies with the cycle length. This has been demonstrated in Appendix (Fig. 12), where we give the wavelet representation of a signal for a small frequency change. To check this result further, we calculated the T(t) function using the ridge extraction techniques developed by Torresani (1995), and obtained the same result (see Fig. 7a).

In the plot of Fig. 7b we show the intensity of the wavelet transform (modulus of wavelet coefficients) tracing the maximum defined before. From Fig. 7 we distinguish several episodes, one corresponding to the Maunder minimum (itself divided in two parts - a deep minimum and the end of the minimum), another corresponding to the Dalton minimum and a small event mentioned above near the year 1900. Within the deep Maunder minimum, our algorithm detects a weak (though hardly significant) signal near $T \sim 30$ years. The three other zones indicated on Fig. 7a correspond to an increase of $T$. There is a time around 1750 where $T$ increases without equivalent decrease of $W(t)$ in Fig. 7b. However, when looking at the initial data (Fig. 3), the first maximum in sunspot group number is significantly smaller than its neighbours. This corresponds to a single 11-year cycle, and thus does not show up in Fig. 7b. We can conclude that before each solar activity minimum $T$ increases, and is accompanied with a low level of solar activity that persists as long as $T$ increases; the deeper the minimum, the higher the $T$ level before the event. Let us stress that the variation of $T$ near 1900 was also associated with a decrease in the strength of the cycle.

The three events mentioned above follows a 100-year periodicity, which produces the second intensive layer seen in Fig. 4 (and the peak in the spectrum on Fig. 5a): this corresponds to the Gleissberg cycle. It is tempting to connect its duration with the typical time intervals between the Maunder minimum, the Dalton minimum and the event near 1900. This idea can be illustrated by using the Mexican hat transform, where white

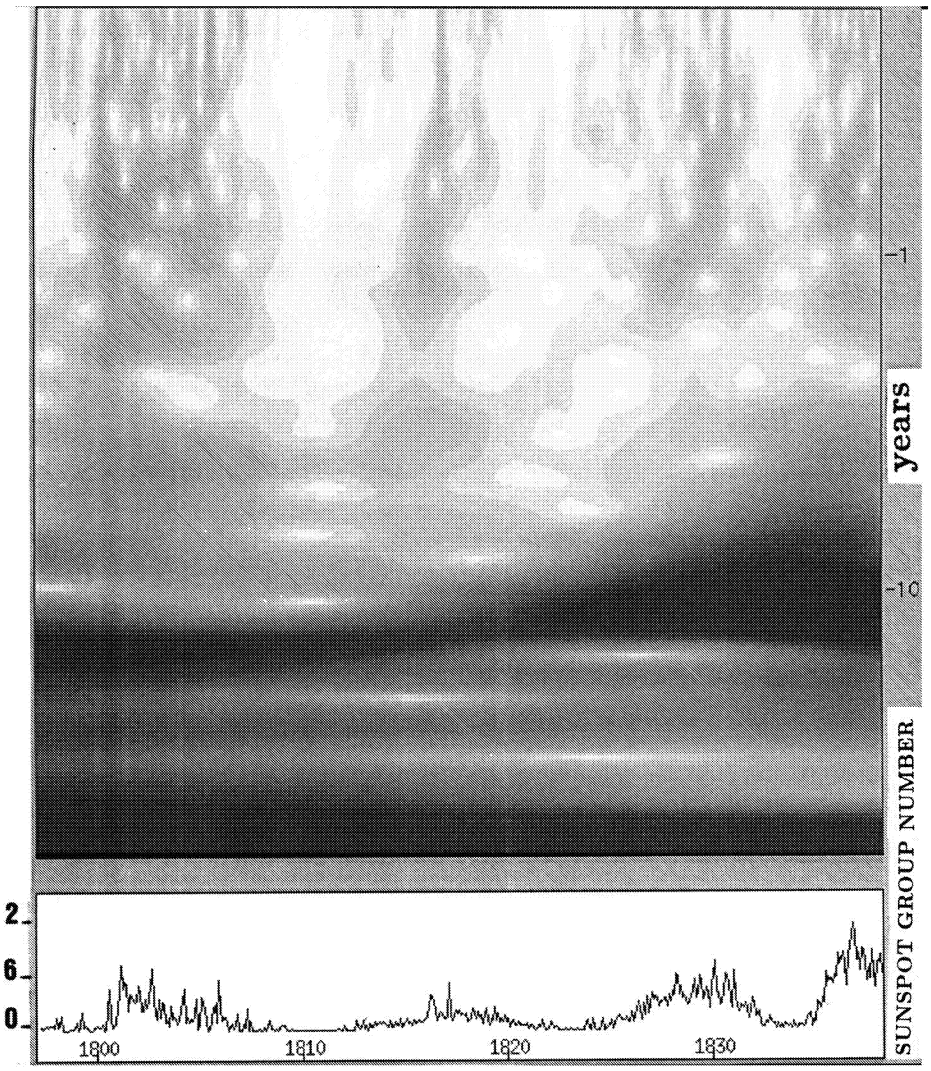


**Fig. 9.** Morlet wavelet transform for the Dalton minimum (1796 – 1845): modulus.

vertical layers isolate epoch of the grand deviations from that of normal activity (Fig. 6). The next deviation should be expected soon since the last one occured about 100 years ago. But no great minimum is to be expected because the level of $T$ corresponding to the present level is not high. Along this line of thought, sunspots of new cycle (cycle 23) have been observed in 1995 and do not exceed 20 degres latitude. This could be an indication that cycle 23 would be weaker than the previous ones.

Physical properties of the grand deviations in terms of sunspot number, asymmetry, and rotation have been studied (Nesme-Ribes et al. 1994), and a possible scenario for the chaotic long-term magnetic evolution has been proposed by Nesme-Ribes et al. (1994).

### *4.3. Wavelet analysis for Maunder minimum-type episodes*

The intensities contrast between the Maunder minimum and nearby epochs is very large (Fig. 4). So we assume that the properties of the grand minimum is somehow reflecting the characteristics of the nearby epoch. This is why we consider several time intervals: the whole Maunder minimum (1643 — 1712), and the end of the Maunder minimum (1695 — 1737). For comparison, we also study the Dalton minimum (1796 — 1845). Results of the wavelet technique are shown for the end of the Maunder minimum (Fig. 8), and for the Dalton minimum (Fig. 9). These events show strong similarities and are characterized by a small increase of the cycle length, with a substantial decrease in the cycle strength. As we consider only monthly sunspot group data, we cannot describe the main features occuring at the end of Maunder minimum, namely the recovery of the north-south symmetry which is typical of the normal state of solar activity (Jennings, 1991; Sokoloff and Nesme-Ribes, 1994).

A quite different result was obtained for the deep Maunder minimum (Figs. 10 and 11). There is no signal corresponding to the Schwabe cycle. Such a specific feature does not appear in any other wavelet transform domain. Suppose that we are dealing with the modulus of a sinusoidal, one or two of the period having a zero value (Appendix). The wavelet transform would produce the same pattern as that seen on Figs. 10 and

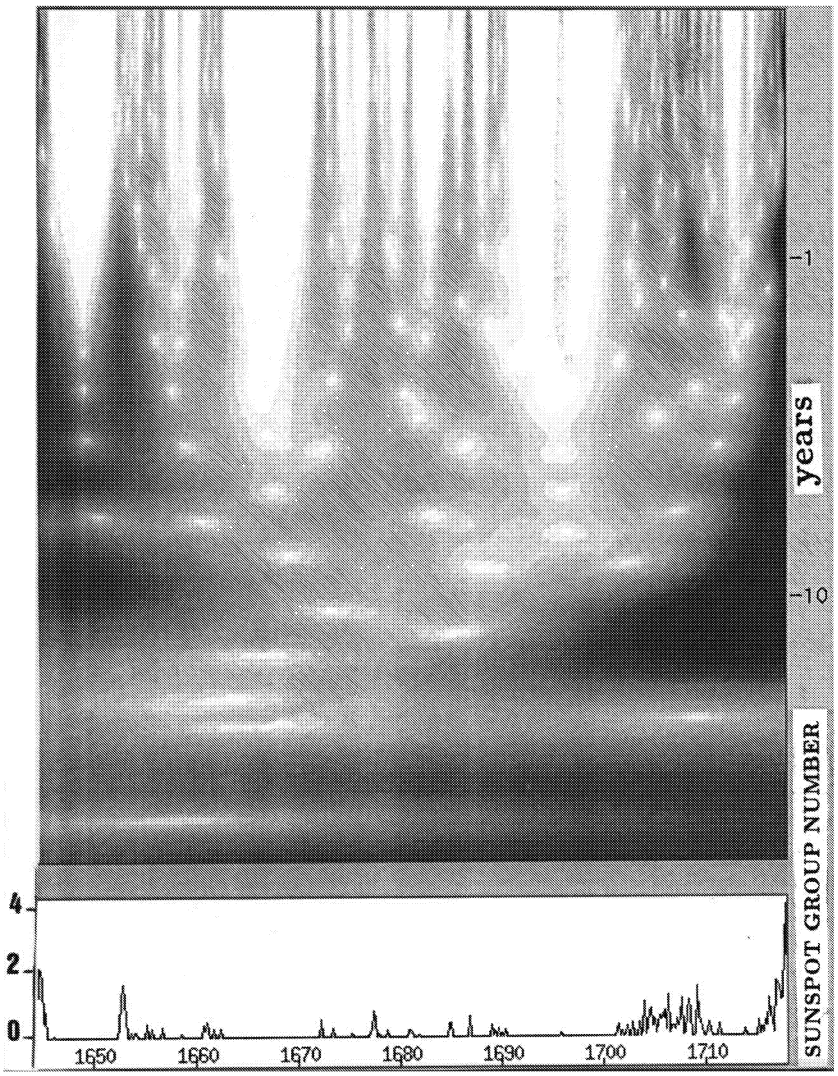


**Fig. 10.** Morlet wavelet transform for the deep Maunder minimum (1643 – 1712): modulus.

11. So our interpretation is that sunspot groups did not show any clear 11-y periodicity during the deep Maunder minimum (1670 — 1690). The sparse sunspots occuring at that time do not follow any periodic process, and should be considered as white noise. The 11-y periodicity was recovered after 1690, at the end of Maunder minimum. Comparison of Figs. 10 to 11 hints that the culmination of events referred to as the Maunder minimum occured near 1665-1670.

## 5. Conclusion and discussion

The properties of the solar activity were studied by means of the wavelet technique. Two typical time scales can be obtained in the wavelet analysis, the 11-year cycle and a 100-y cycle.

Furthermore, our analysis shows that there are three events over the last four centuries which show deviations from the normal activity state. One of them results in the well-known Maunder minimum which is the largest minimum observed so far on the Sun, while the other two show local deviations to a lesser degree. These smaller deviations can be compared with the solar activity observed at the end of the deep Maunder minimum (after 1690). Additional evidence of the recovery of solar activity at the end of Maunder minimum is visible in other properties of solar activity, namely the asymmetry of the butterfly diagram and the extension of its wings, the solar rotation rate (Ribes and Nesme-Ribes, 1993; Sokoloff and Nesme-Ribes, 1994). The abrupt transition from active cycles to a grand minimum and the recovering of solar activity have been investigated numerically in the framework of dynamo theory by Brandenburg et al. (1989, 1991).

Other events that show up in the wavelet analysis are the Dalton minimum and an event near 1900. Two of these minima have been mentioned by Ochadlick et al. (1993). However, they are much less visible in their wavelet analysis as they were using yearly sunspot numbers.

One important finding is the existence of two parts within the Maunder minimum: a deep minimum with no cyclic sunspot production, and the end of the Maunder minimum with a resumption of the Schwabe cycle. The transition between the stages is abrupt.

We studied the length-strength correlations of the 11-y cycle, and showed that the decrease in solar activity coincides with

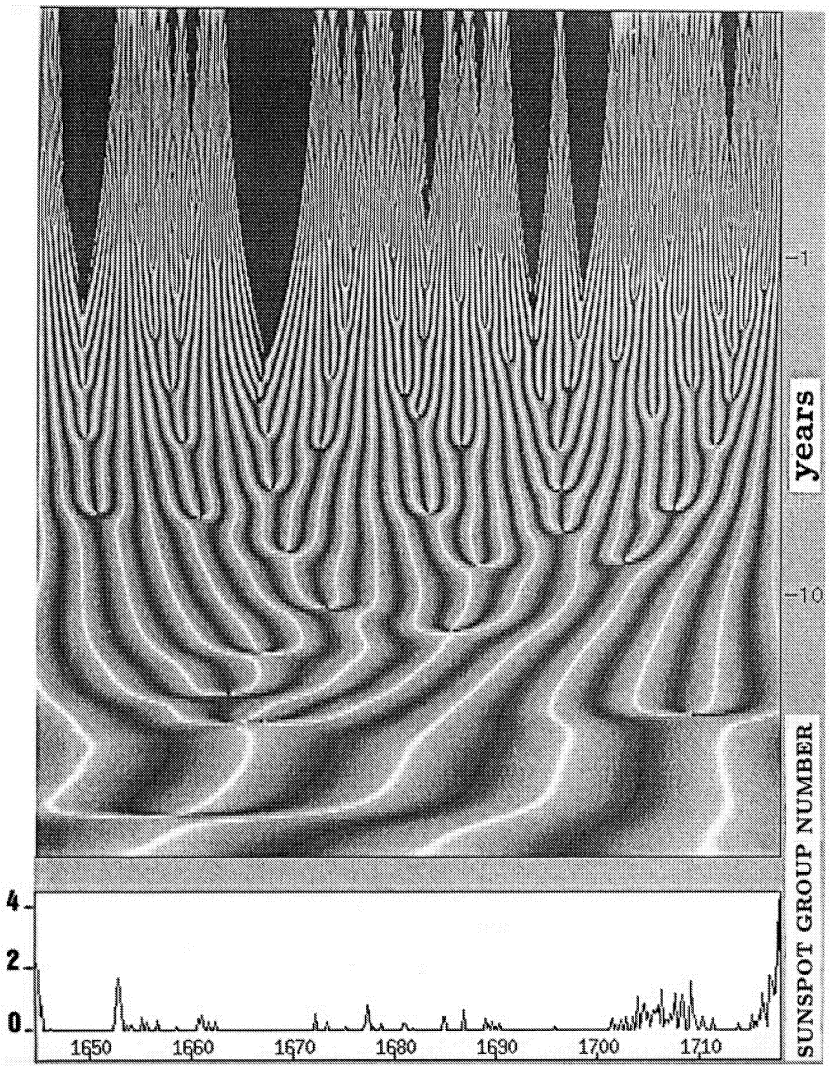


**Fig. 11.** Morlet wavelet transform for the deep Maunder minimum (1643 – 1712): phase.

the negative derivative of the cycle length ($T$): the weaker the amplitude the longer the period.

The absence of sunspot cycle during the deep Maunder minimum raises the question of whether or not the dynamo mechanism was operating during this period. An 11-year periodicity was detected in the $C^{14}$ data throughout the Maunder minimum (Stuiver and Braziunas, 1993) as well as by wavelet analysis of historical solar diameter data (Nesme-Ribes et al., 1995), thereby suggesting that the periodic dynamo was still at work. On the other hand, an oscillatory toroidal magnetic field embedded deep in the Sun can produce sunspots provided the field strength is large enough. So one possible explanation is that the toroidal magnetic field was too weak to create sunspots.

*Acknowledgements.* We are grateful to B. Torresani for his help in providing an algorithm to ridge extraction. Our thanks go to Marie Farge and B. Torresani for helpful discussions and improvments of the paper.

The financial support of the Russian Found of Basical Researches under grants 94-01-00951-a, 96-02-16252a and 95-02-03724, 97-05-64797 is gratefully acknowledged. The numerical simulations were made possible by grants from the Swedish Royal Academy of Science, Eriksson foundation, and material support from NADA (Royal Institute of Technology, Stockholm). E. N-R and D.S are grateful to DRET (contrat 92-20011.A) and C.N.R.S.

## Appendix

The most popular canonical example (see e.g. Farge, 1992) is a frequency doubling in a harmonic signal. Here, we present the Morlet wavelet transform of a harmonic (11-y period) signal with a relatively small frequency change ($\Delta\omega/\omega_0 = 0.1$) at $t = t_0$ (Figs. 12 and 13).

We also examine the Morlet wavelet transform $w(a, t)$ for a harmonic (11-y period) signal exhibiting a 1-y phase shift ($\Delta\phi = \pi/10$) (Figs. 14 and 15).

The third canonical example aims at illustrating Maunder minimum-type events. For that, we examine the modulus of a periodic signal that contains a gap of two oscillations (Figs. 16 and 17).

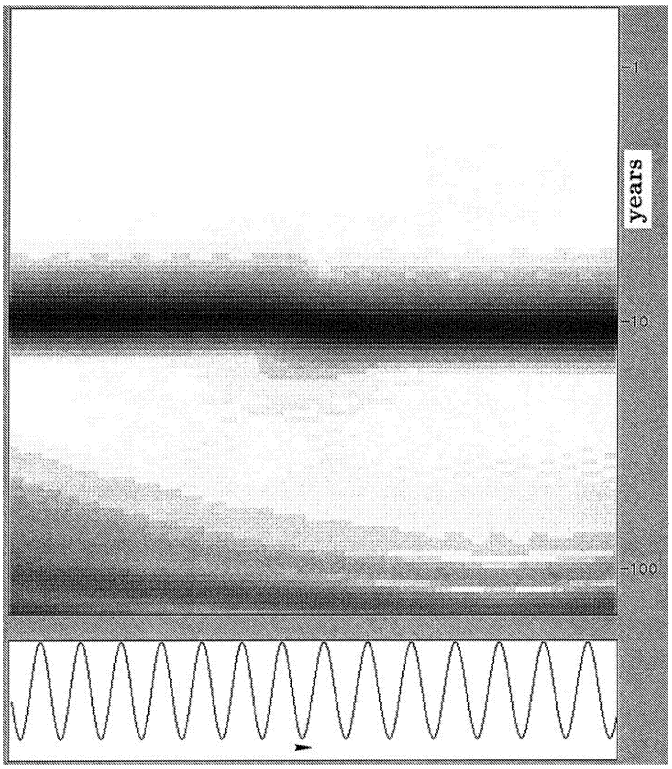


**Fig. 12.** Canonical example of a Morlet wavelet transform: the sinusoidal period increases from 11 to 12 years. Modulus

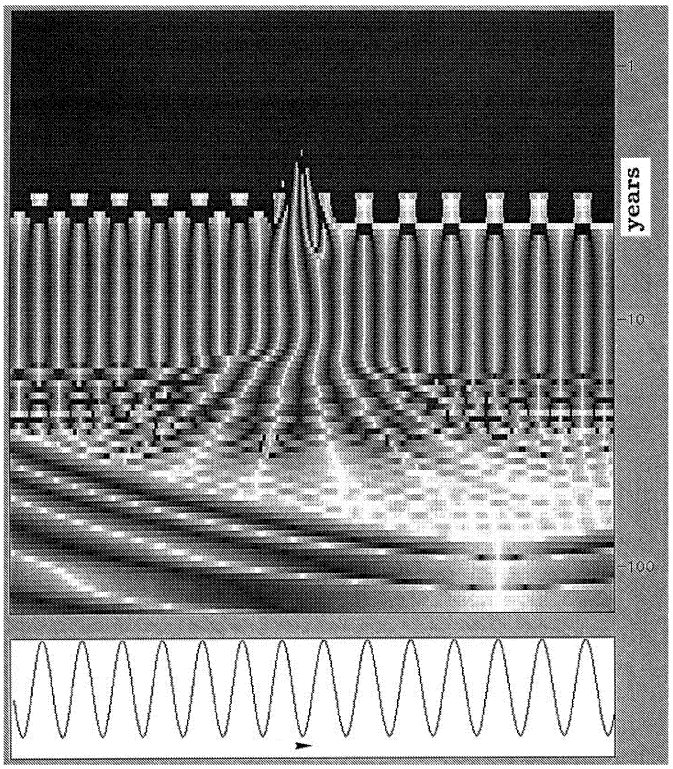


**Fig. 13.** Canonical example of a Morlet wavelet transform: the sinusoidal period increases from 11 to 12 years. Phase

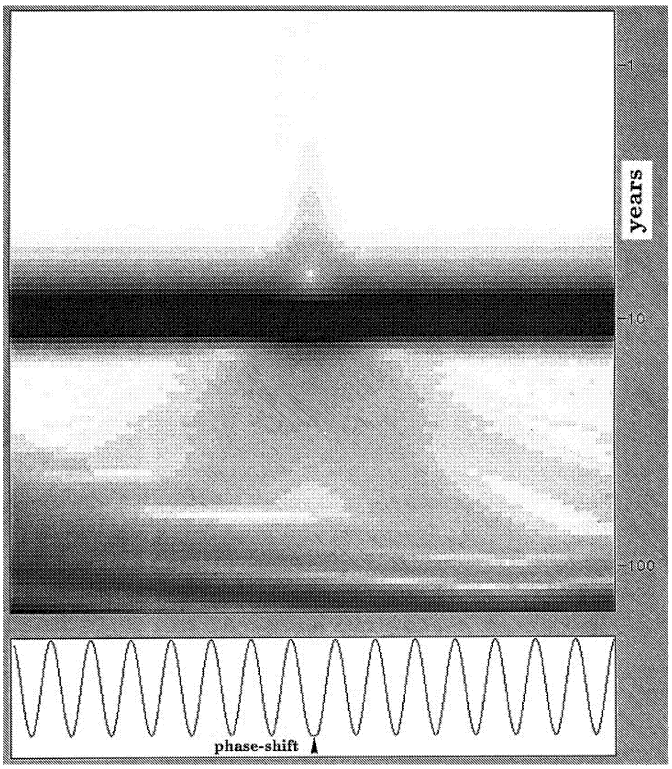


**Fig. 14.** Canonical example of a Morlet wavelet transform: the sinusoidal phase is shifted by $\Delta\phi = -\frac{2\pi}{11}$. Modulus

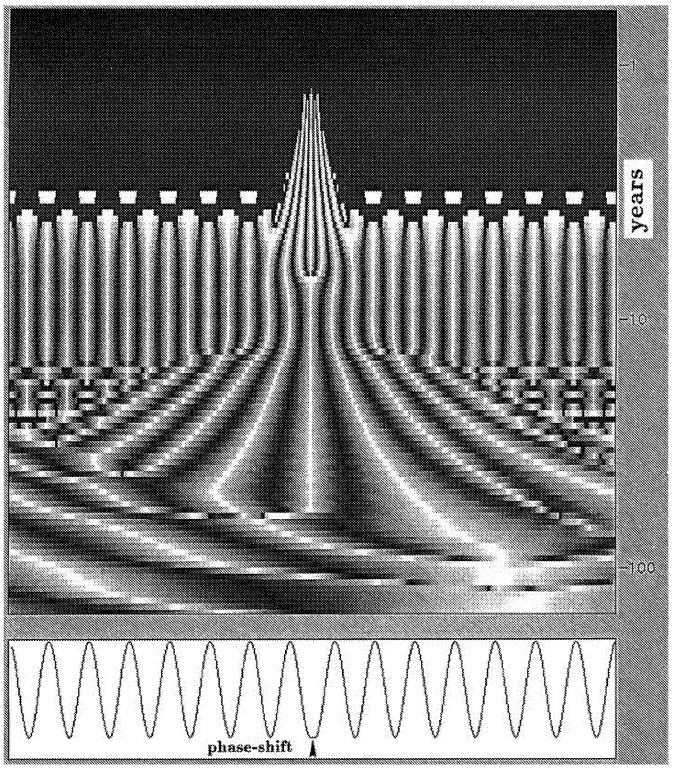


**Fig. 15.** Canonical example of a Morlet wavelet transform: the sinusoidal phase is shifted by $\Delta\phi = -\frac{2\pi}{11}$. Phase.

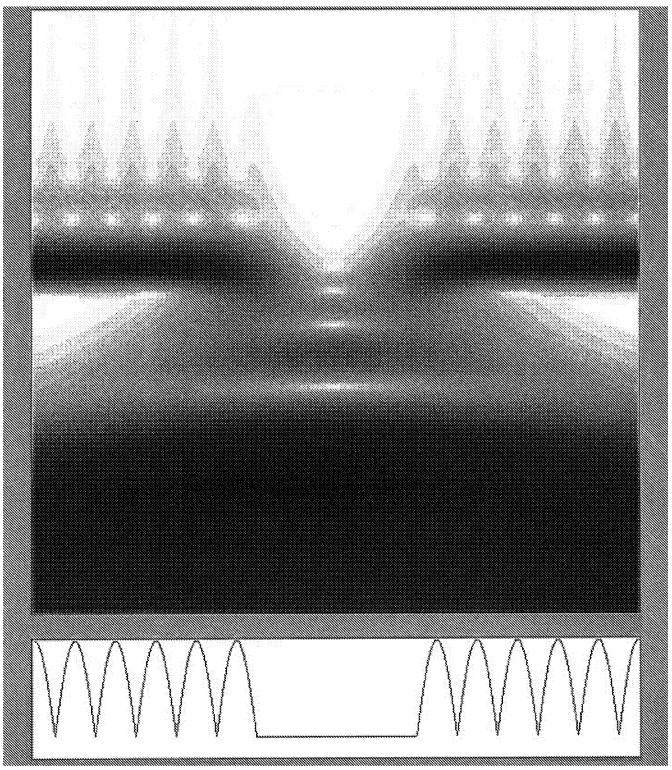

**Fig. 16.** Morlet wavelet transform for an artificial example: modulus of sinusoidal with a gap of two oscillations; modulus of wavelet coefficients.

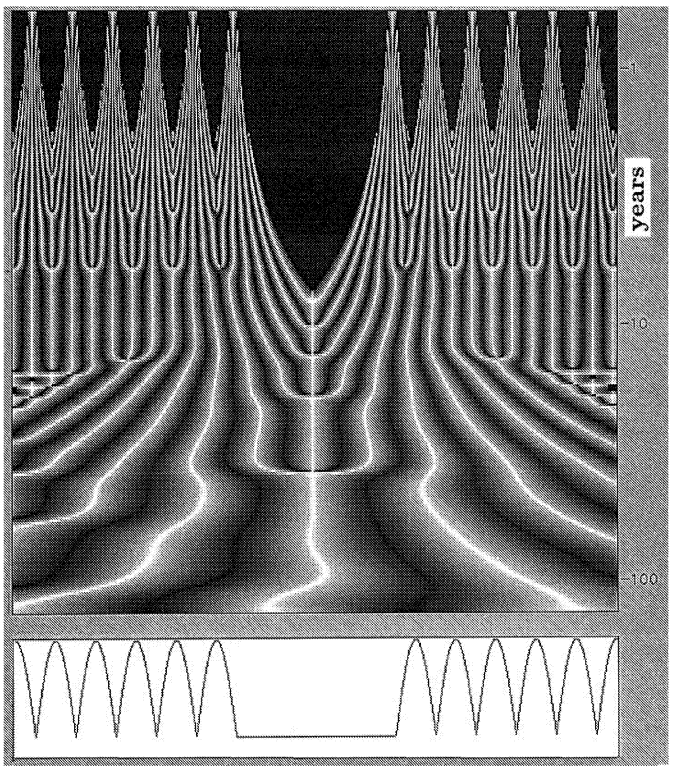


**Fig. 17.** Morlet wavelet transform for an artificial example: a sinusoidal with a gap of two oscillations; phase.

## References


Altarac, S., 1995, Analyse Temps-Fréquence de données astronomiques, Rapport de stage, Institut de Physique et chimie Industrielle, (Lyon), 19

Brandenburg A., Krause F., Tuominen I., 1989, in Meneguzzi M., Pouquet A., Sulem P.L.(eds), MHD Flows, p. 35.

Brandenburg A., Krause F., Meinel L., Tuominen I., 1991, A&A 213, 241

Daubechies I., 1992 Ten lectures on wavelets, SIAM, Philadelphia

Donoho, D.L., 1994, Wavelets: theory, Algorithms and Applications, ed. C.K. Chui, L. Montefusco and L. Puccio, 233

Farge M., 1992, Ann. Rev. Fluid Mech. 24, 395

Hoyt D.V., Schatten K.H., 1992a, ApJ 384, 361

Hoyt D.V., Schatten K.H., 1992b, Solar Phys. 138, 387

Hoyt D.V., Schatten K.H., Nesme-Ribes E., 1994, Geophys. Res. Let. 21, 2067

Grossmann A., Morlet J., 1984, SIAM J.Math.Anal. 15, 723.

Jennings R.L., 1991, GAFD 57, 147

Lawrence J.K., Cadavid A.C., Ruzmaikin A.A., 1995, ApJ 455, 366

Meyer Y., Wavelets and operators, Cambridge, 1992

Nesme-Ribes E., Frick P., Sokoloff D., Zakharov V., Ribes J.-C., Vigouroux A., Laclare F., 1995, C.R. Acad. Sci. Paris 321, II, 525

Nesme-Ribes E., Sokoloff D., Ribes J.C., Kremliovsky M., 1994, in Nesme-Ribes E. (ed.) The Solar Engine and Its Influence on Terrestrial Atmosphere and Climate, 71.

Ochadlick A.R., Kritikos H.N., Giegengack R., 1993, Geophys. Res. Lett. 20, 1471

Perrier V., Philipovitch T. and Basdevant C., 1995, J. Math. Phys. 36 (3), 1506

Ribes E., Merlin, Ph., Ribes, J.C., and Barthalot, R., 1989, Annales geophysicae 7, 321

Ribes J.C., Nesme-Ribes E., 1993, A&A 276, 549

Sokoloff D., and Nesme-Ribes E., 1994, A&A 288, 293

Soon W.H., Baliunas S.L., Zhang Q., 1994, Solar Phys. 154, 385

Stuiver M., and Braziunas T., 1993, The Holocene, 3, 4, 289

Torresani, B., 1995, Analyse continue par ondelettes, Inter-editions, Savoir Actuels

Wolf R., 1851, Naturf. Gesell. Bern. Mitt. 1, 89


This article was processed by the author using Springer-Verlag LaTeX A&A style file *L-AA* version 3.